metals

MDPI

Article

External-Field-Induced Phase Transformation and Associated Properties in a $Ni_{50}Mn_{34}Fe_3In_{13}$ Metamagnetic Shape Memory Wire

Zhen Chen [1], Daoyong Cong [1,*], Shilei Li [1], Yin Zhang [1], Shaohui Li [1], Yuxian Cao [1], Shengwei Li [1], Chao Song [1], Yang Ren [2] and Yandong Wang [1]

[1] Beijing Advanced Innovation Center for Materials Genome Engineering, State Key Laboratory for Advanced Metals and Materials, University of Science and Technology Beijing, Beijing 100083, China; b20160442@xs.ustb.edu.cn (Z.C.); lishilei@ustb.edu.cn (S.L.); yinzhang330@163.com (Y.Z.); b20160443@xs.ustb.edu.cn (S.L.); b20190501@xs.ustb.edu.cn (Y.C.); b20200522@xs.ustb.edu.cn (S.L.); b20180487@xs.ustb.edu.cn (C.S.); ydwang@ustb.edu.cn (Y.W.)

[2] X-ray Science Division, Argonne National Laboratory, Argonne, IL 60439, USA; ren@aps.anl.gov

* Correspondence: dycong@ustb.edu.cn; Tel.: +86-10-6233-2508

Abstract: Metamagnetic shape memory alloys exhibit a series of intriguing multifunctional properties and have great potential for applications in magnetic actuation, sensing and magnetic refrigeration. However, the poor mechanical properties of these alloys with hardly any tensile deformability seriously limit their practical application. In the present work, we developed a Ni-Fe-Mn-In microwire that exhibits both a giant, tensile superelasticity and a magnetic-field-induced first-order phase transformation. The recoverable strain of superelasticity is more than 20% in the temperature range of 233–283 K, which is the highest recoverable strain reported heretofore in Ni-Mn-based shape memory alloys (SMAs). Moreover, the present microwire exhibits a large shape memory effect with a recoverable strain of up to 13.9% under the constant tensile stress of 225 MPa. As a result of the magnetic-field-induced first-order phase transformation, a large reversible magnetocaloric effect with an isothermal entropy change ΔS_m of 15.1 J kg^{-1} K^{-1} for a field change from 0.2 T to 5 T was achieved in this microwire. The realization of both magnetic-field and tensile-stress-induced transformations confers on this microwire great potential for application in miniature multi-functional devices and provides an opportunity for multi-functional property optimization under coupled multiple fields.

Keywords: metamagnetic shape memory alloy; microwire; superelasticity; martensitic transformation; magnetocaloric effect; magnetic-field-induced phase transformation; magnetostructural transformation; shape memory effect

Citation: Chen, Z.; Cong, D.; Li, S.; Zhang, Y.; Li, S.; Cao, Y.; Li, S.; Song, C.; Ren, Y.; Wang, Y. External-Field-Induced Phase Transformation and Associated Properties in a $Ni_{50}Mn_{34}Fe_3In_{13}$ Metamagnetic Shape Memory Wire. *Metals* **2021**, *11*, 309. https://doi.org/10.3390/met11020309

Academic Editor: Ryosuke Kainuma
Received: 14 January 2021
Accepted: 5 February 2021
Published: 10 February 2021

1. Introduction

Shape memory alloys (SMAs), as a unique class of smart materials, which combine the functional properties such as shape memory effect (SME), superelasticity (SE) and elastocaloric effect, have drawn great attention in recent years [1,2]. The underlying mechanism of these properties is a reversible phase transformation between a high-temperature austenitic phase and a low-temperature martensitic phase when an external stimulus of stress or temperature is applied [3]. Thus, SMAs show great potential for application as actuators and sensors in industrial [4,5], automotive [2,6], aerospace [3,7], micro-electromechanical system (MEMS) [8] and biomedical [9] fields. For the majority of actuators and sensors, fast response and large output strain/stress are imperative and desirable properties. Metamagnetic shape memory alloys (MMSMAs) have provoked much interest in recent years due to their high response frequency and output stress arising from the strong coupling of crystal and magnetic structures. In these alloys, it is possible to obtain such multifunctional properties as magnetic superelasticity [10,11], magnetic shape memory effect [12], magnetoresistance [13] and magnetocaloric effect [14–16].

In principle, MMSMAs can display a phase transformation under an external field of magnetic field, stress or temperature and optimized multifunctional properties can be anticipated under the coupling of magnetic field, stress and temperature. Unfortunately, polycrystalline MMSMAs show intrinsic brittleness, as a result of deformation and transformation incompatibility at grain boundaries and triple junctions [17], which severely limits their practical application. Moreover, it is difficult for these alloys to serve under the condition of the simultaneous application of magnetic field and stress in order to exhibit optimized multifunctional properties because they can easily fracture under external stress due to their high brittleness. It is of great importance to develop MMSMAs with good mechanical properties so that they can bear a high enough stress for stress-induced martensitic transformation.

Recently, it was proposed that the deformation and transformation incompatibility at grain boundaries and triple junctions in SMAs could be diminished by reducing their dimensions [18]. Low-dimension SMAs (particles, wires, films, ribbons, micropillars or foams) exhibit great application potential in micro-actuators or micro-sensors. This is due to the high ratio of surface to volume, which could improve the response speed [8,19]. The Taylor–Ulitovsky [20,21] and melt-extraction [22] methods are two feasible and easy methods to produce magnetic shape memory microwires. The Taylor–Ulitovsky method, which involves rapid solidification and drawing, is prone to produce microwires with an oligocrystalline structure. This structure reduces the incompatibility between different grains and thus effectively enhances the mechanical properties of Ni-Mn-based MMSMAs [23,24]. Although scattered attempts have been made to investigate the external-field-induced transformation of Ni-Mn-based MMSMA microwires that were prepared using this method, the reported microwires with a magnetic-field-induced transformation exhibit a limited recoverable strain of superelasticity and those with a large recoverable strain barely display magnetic-field-induced transformation. Therefore, there is an urgent need to develop high-performance MMSMAs with both a giant recoverable strain and a magnetic-field-induced first-order phase transition.

In the present work, we successfully developed a Ni-Mn-Fe-In MMSMA microwire exhibiting a giant, tensile superelasticity with a recoverable strain higher than 20%. Furthermore, the microwire shows a magnetic-field-induced first-order phase transformation and a reversible isothermal magnetic entropy change of 15.1 J kg^{-1} K^{-1} for a field change from 0.2 T to 5 T. The simultaneous achievement of a magnetic-field-induced phase transformation and a giant, tensile recoverable strain confers on this microwire great potential for application in miniature multifunctional devices.

2. Materials and Methods

$Ni_{50}Mn_{34}Fe_3In_{13}$ (at. %) polycrystalline button ingots were prepared by arc melting the pure Ni, Mn, Fe, and In elements. The ingots were melted four times in order to ensure homogeneity. The Taylor–Ulitovsky method [20,21] was used to prepare the glass-coated microwires with a diameter of 50−150 μm. After removing the glass sheath, the microwires were tested without any post heat treatments. The cross-section and surface morphologies of the microwire were investigated using a scanning electron microscope (SEM, Carl Zeiss, Oberkochen, Germany). The crystallographic orientation was studied using electron backscatter diffraction (EBSD, Carl Zeiss, Oberkochen, Germany), which was conducted at room temperature in the SEM. Synchrotron high-energy X-ray diffraction (HEXRD) experiments were conducted using a monochromatic X-ray beam with a wavelength of 0.1173 Å at the 11-ID-C beam line of the Advanced Photon Source at the Argonne National Laboratory, USA.

Mechanical tests were conducted in tension using a dynamic mechanical analyzer (DMA, TA Instruments, New Castle, DE, USA) with a maximum load of 18 N equipped with a closed furnace. The stress–strain curves were measured by force control at a loading–unloading rate of 50 MPa/min. The force was measured by using a load cell with a high resolution (10^{-5} N). The strain was determined by cross-head displacement using a high-

resolution linear optical encoder that has a displacement resolution of 1 nm. The total length and gauge length of the samples for mechanical tests were about 12.2 mm and 7.0 mm, respectively. Magnetization as a function of temperature ($M(T)$) under constant magnetic fields and magnetization as a function of magnetic field ($M(H)$) at constant temperatures were measured by a physical property measurement system (PPMS, Quantum Design, San Diego, CA, USA). The $M(H)$ curves were measured by the standard loop process at different constant temperatures during two consecutive cycles of increasing the field to 5 T and then decreasing the field to 0 T. Before measuring the $M(H)$ curves at each temperature, the microwire was cooled to 135 K. This temperature was held for 1 min and then increased to the test temperature. The mass of the samples for the $M(T)$ and $M(H)$ measurements was 1.41 mg.

3. Results

3.1. Microstructure and Crystal Structure

Figure 1a shows the cross-section morphology of the $Ni_{50}Mn_{34}Fe_3In_{13}$ microwire, which indicates that the microwire had a regular, circular cross-section. The surface morphology of the $Ni_{50}Mn_{34}Fe_3In_{13}$ microwire is displayed in Figure 1b, which demonstrates that the microwire had a smooth surface and uniform diameter. The EBSD orientation map of the $Ni_{50}Mn_{34}Fe_3In_{13}$ wire was measured at room temperature and is shown in Figure 1c. No obvious grain boundaries can be observed in the sample used for EBSD measurement. This implies that the constraints of grain boundaries have been much reduced in the microwire—the grain size was as large as several millimeters [23].

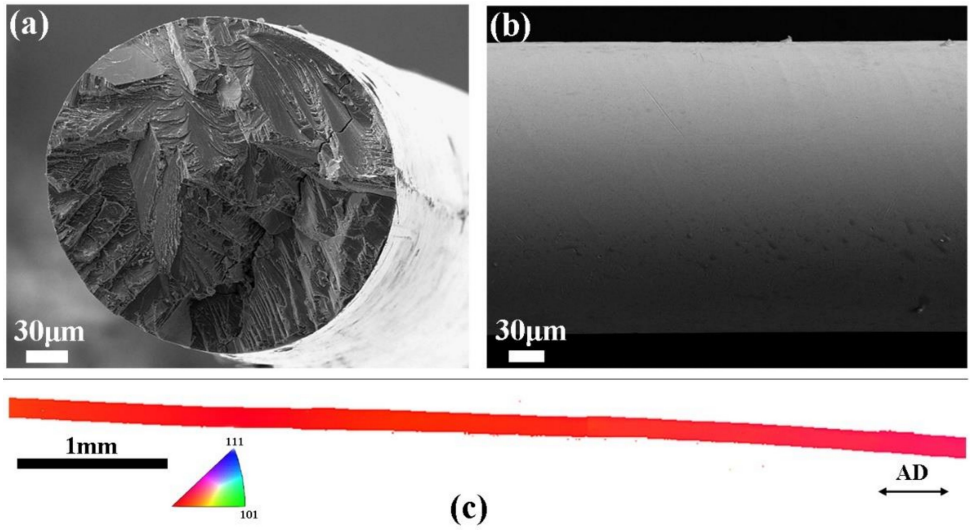

Figure 1. Microstructure of the $Ni_{50}Mn_{34}Fe_3In_{13}$ microwire at room temperature. (**a**,**b**) SEM images of the cross-section (**a**) surface (**b**); (**c**) Electron backscatter diffraction (EBSD) orientation map presented in inverse pole figure mode; the legend of a stereographic triangle (parallel to the wire axis direction AD) is also shown.

Figure 2a,b show the HEXRD patterns recorded at 298 K and 110 K, respectively, during the cooling of the $Ni_{50}Mn_{34}Fe_3In_{13}$ microwire. The crystal structures of austenite and martensite were identified with the help of the software PowderCell [25]. The pattern collected at 298 K in Figure 2a can be well indexed according to the cubic $L2_1$ Heusler structure (space group $Fm\bar{3}m$, No. 225) with lattice parameter a_A = 5.970 Å. As can be seen, besides the strong diffraction peaks of (220), (422) and (400), the superlattice reflections of (111), (311) and (331) can also be observed (see the inset of Figure 2a), which are characteristic of the $L2_1$ structure. At 110 K, the main diffraction peaks in Figure 2b can be well indexed according to the six-layered modulated (6M) structure of martensite (space group $P2/m$, No. 10) with lattice parameters a_{6M} = 4.395 Å, b_{6M} = 5.622 Å, c_{6M} = 25.824 Å and β = 92.10°. However, several other small peaks can also be seen in Figure 2b. These

small peaks can be well indexed according to the cubic $L2_1$ structure of austenite with lattice parameter a_A = 5.955 Å. This implies that a tiny amount of austenite was retained at this temperature.

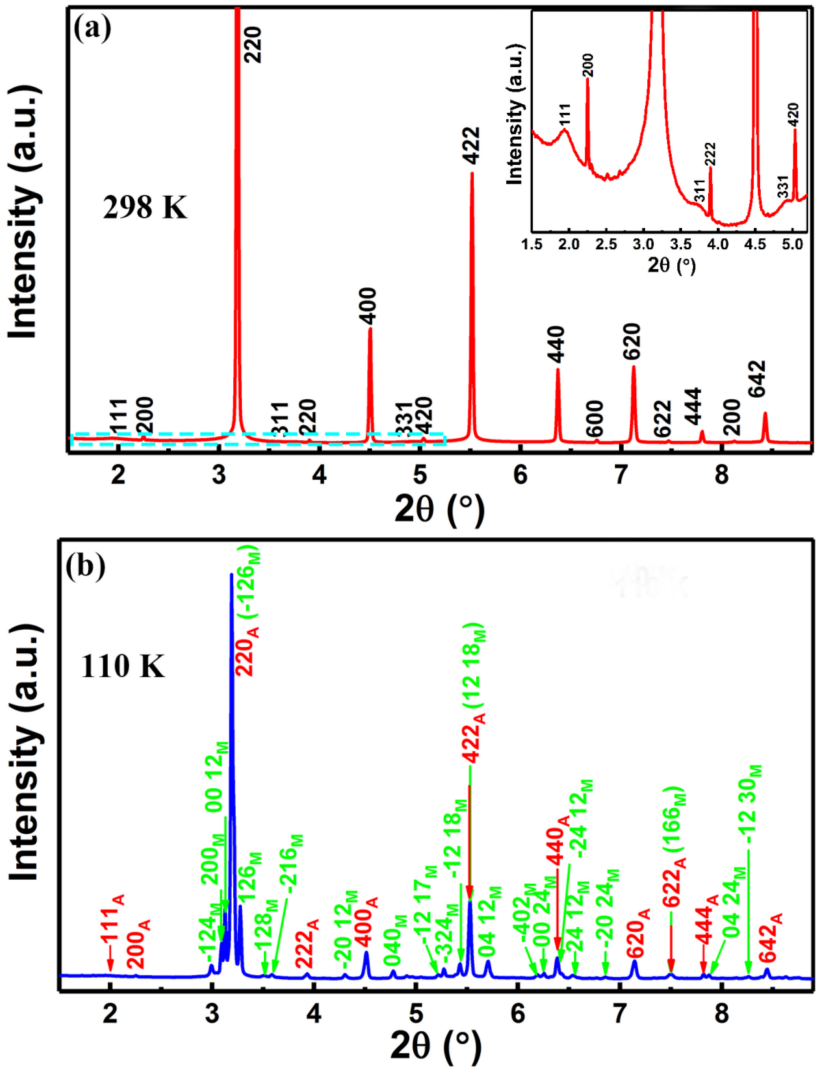

Figure 2. High-energy X-ray diffraction (HEXRD) patterns recorded at the temperatures of (**a**) 298 K and (**b**) 110 K for the $Ni_{50}Mn_{34}Fe_3In_{13}$ microwire. The inset in (**a**) displays the magnified view of the pattern in the 2θ range of 1.5–5.5°. "A" and "M" in the indices in (**b**) denote austenite and martensite, respectively.

Based on the geometric nonlinear theory of martensite, it is possible to evaluate the geometric compatibility between martensite and austenite. The middle eigenvalue λ_2 of the transformation stretch matrix **U**, which is used to characterize the geometric compatibility, can be computed with the algorithms reported in [26,27]. With the lattice parameters of austenite and martensite determined above, the λ_2 for the $Ni_{50}Mn_{34}Fe_3In_{13}$ microwire was determined to be 1.0083, which is close to 1. This implies a good geometric compatibility between martensite and austenite, which could explain the small thermal hysteresis of 8.9 K in the present microwire. This is because good geometric compatibility usually leads to a small thermal hysteresis [26].

3.2. Stress-Induced Phase Transformation and Superelasticity

In order to study the superelasticity that results from stress-induced martensitic transformation in the microwire, stress–strain curves at different constant temperatures

were recorded. Figure 3a displays the tensile stress–strain curves at different constant temperatures in the temperature range of 213–283 K for the $Ni_{50}Mn_{34}Fe_3In_{13}$ microwire. The determination of the critical stress for stress-induced martensitic transformation σ_{cr}, stress hysteresis of the stress-induced martensitic transformation $\Delta\sigma$, irrecoverable strain after unloading ε_{irr}, superelastic strain ε_{se} and elastic strain ε_{el}, is illustrated in Figure 3b. In Figure 3a, at 213 K, two stress plateaus can be observed during loading, which indicated that inter-martensitic transformation occurred at this temperature. An irrecoverable strain ε_{irr} of 1.3% was observed after unloading when the maximum applied strain was 21.1%. This may be because a small amount of stress-induced martensite was stabilized and failed to transform back to austenite after unloading, as the test temperature (213 K) was slightly higher than the austenite transformation finish temperature A_f. This conjecture was confirmed by the recovery of the strain (1.3%) after heating to a higher temperature of 233 K. Encouragingly, the microwire exhibits excellent tensile superelasticity with almost no residual strain after unloading at higher temperatures (in the range between 233 and 283 K). Strikingly, a giant recoverable strain ε_{rec} of 20.3% was achieved in this temperature range, which is the highest recoverable strain reported so far in Ni-Mn-based SMAs. This value is much higher than that of Ni-Ti wire (approximately 11.5%), which is used for practical applications at present [28]. The temperature dependence of the critical stress for stress-induced martensitic transformation σ_{cr} is shown in Figure 3c. It can be seen that the critical stress increased linearly with the increase of temperature at a rate of 1.69 MPa/K.

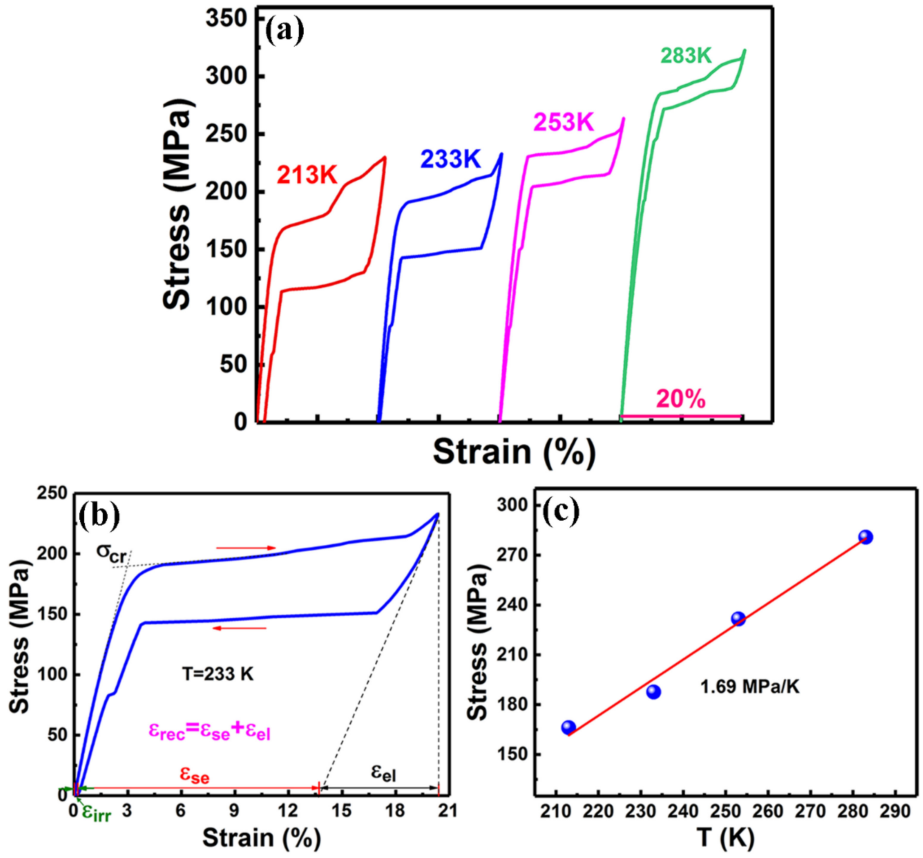

Figure 3. (**a**) Tensile stress–strain curves recorded at different constant temperatures in the range of 213–283 K for the $Ni_{50}Mn_{34}Fe_3In_{13}$ microwire. (**b**) Tensile stress–strain curve measured at 233 K with the determination of the following parameters: the critical stress for stress-induced martensitic transformation σ_{cr}, the stress hysteresis of the stress-induced martensitic transformation $\Delta\sigma$, the irrecoverable strain after unloading ε_{irr}, the superelastic strain ε_{se} and the elastic strain ε_{el}. The total recoverable strain ε_{rec} is the sum of ε_{se} and ε_{el}. (**c**) Temperature dependence of the critical stress for stress-induced martensitic transformation σ_{cr}.

The shape memory effect was examined by load-biased thermal cycling tests under different constant stresses. The strain–temperature curves recorded under stress levels of 25, 75, 125 and 225 MPa for the $Ni_{50}Mn_{34}Fe_3In_{13}$ microwire are shown in Figure 4. The recoverable strain ε_{rec} and irrecoverable strain ε_{irr} were determined and are illustrated in the figure. As can be seen, the strain associated with martensitic transformation was completely recovered after the cooling–heating cycle when the applied stresses were not higher than 75 MPa. The recoverable strains were high; they were 5.0% under 25 MPa and 8.9% under 75 MPa. The irrecoverable strain ε_{irr} occurred when the stress increased to above 125 MPa. In spite of this, ε_{rec} continued to increase as the stress increased, and amounted to 9.5% under 125 MPa. Strikingly, when the stress increased to 225 MPa, a ε_{rec} as high as 13.9% was achieved. This is the highest shape memory strain that has been reported to date in Ni-Mn-based SMAs, which is of great importance to realizing a large stroke in actuator applications [2,29].

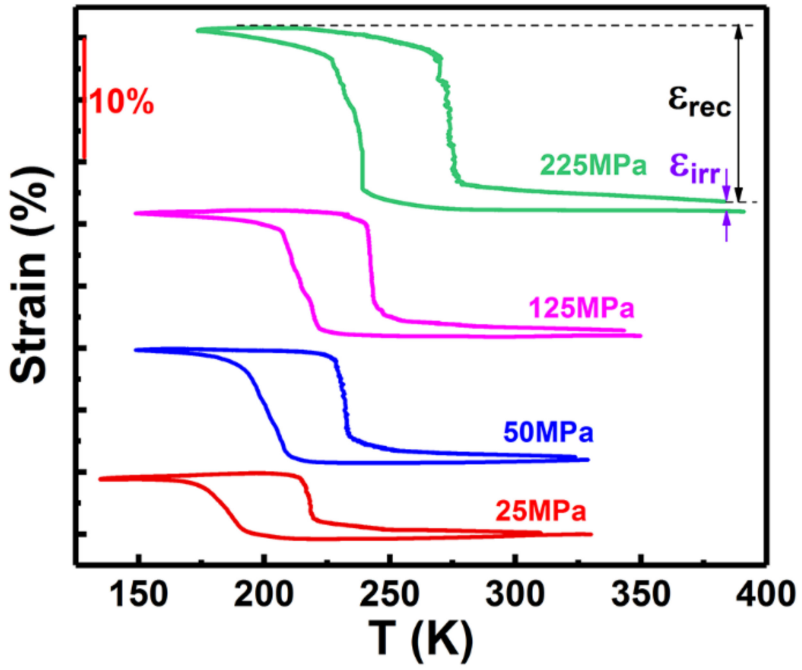

Figure 4. Strain–temperature curves measured under different constant stresses for the $Ni_{50}Mn_{34}Fe_3In_{13}$ microwire.

3.3. Magnetic-Field-Induced Phase Transformation and Magnetocaloric Effect

In order to study the magnetic properties of the $Ni_{50}Mn_{34}Fe_3In_{13}$ microwire, the $M(T)$ curves were measured. The $M(T)$ curves measured under 0.05 T and 5 T are shown in Figure 5a. As can be seen, the high-temperature austenitic phase and low-temperature martensitic phase are ferromagnetic and weak magnetic, respectively. During cooling, a major part of the austenite transformed into martensite when the temperature range was: (1) between 184 K and 182 K under 0.05 T; and (2) between 164 K and 162 K under 5 T, respectively. Upon further cooling, the remaining austenite continuously and gradually transformed into martensite. The dM/dT as a function of temperature, which is derived from the $M(T)$ curves in Figure 5a, is illustrated in Figure 5b. The martensitic transformation temperature (T_M) and the reverse transformation temperature (T_A) were determined by the temperatures corresponding to the maximum dM/dT values during cooling and heating, respectively. The T_M under the magnetic fields of 0.05 T and 5 T were 182.7 K and 162.2 K, respectively, while the T_A under 0.05 T and 5 T were 197.8 K and 178.3 K, respectively. As can be seen from Figure 5b, all the phase transformation temperatures decreased under 5 T when compared to those under 0.05 T. This may be due to the stabilization of austenite with a higher magnetization by the applied magnetic field. Specifically, T_A decreased by 19.5 K

when the applied field was 5 T. Thus, the magnetic field dependence of T_A, $\Delta T_A/\mu_0\Delta H$, was −3.94 K/T.

The change in transformation temperature (ΔT_A) induced by the change in magnetic field ($\mu_0\Delta H$) usually follows the Clausius–Clapeyron relation [12,30,31]:

$$\frac{\Delta T_A}{\mu_0 \Delta H} = -\frac{\Delta M}{\Delta S_{tr}} \quad (1)$$

The transformation entropy change ΔS_{tr} estimated from the endothermic peak of the reverse transformation from the differential scanning calorimetry curve (not shown here) is 18.1 J kg^{-1} K^{-1}. The magnetization difference ΔM obtained from the $M(T)$ curve under 5 T was 68.0 A m^2 kg^{-1}. Therefore, $\Delta M/\Delta S_{tr}$ is 3.76 K/T, which is consistent with the experimental value of $\Delta T_A/\mu_0\Delta H$ (3.94 K/T). The obvious decrease in phase transformation temperatures indicated that a metamagnetic first-order phase transformation from martensite to austenite could be induced if a magnetic field was applied at a temperature that was close to the reverse transformation temperature.

To verify if the magnetic-field-induced phase transformation could occur in the $Ni_{50}Mn_{34}Fe_3In_{13}$ microwire and to examine the reversibility of the transformation, the $M(H)$ curves at different temperatures were measured. The $M(H)$ curves measured during two cycles of ascending and descending magnetic fields at different temperatures in the range 166–186 K are shown in Figure 5c. The thin lines and thick lines represent the first cycle and the second cycle of the ascending and descending magnetic fields, respectively. A rapid increase in magnetization was observed in the initial low-field range (below 0.2 T) at all the test temperatures. This may be due to the initial coexistence of weak magnetic martensite and a small amount of ferromagnetic austenite before the magnetic field was applied. As the magnetic field further increased, a jump in magnetization was observed at the critical field $\mu_0 H_{cr}$, particularly in the temperature range 178–186 K. This phenomenon implies that a strong metamagnetic first-order phase transformation from weak magnetic martensite to ferromagnetic austenite can be induced by the magnetic field. It is worth mentioning that the critical field $\mu_0 H_{cr}$ decreased as the temperature increased. Figure 5c indicates that only a portion of the phase transformation was induced under the magnetic field of 5 T at 166 K and 175 K. However, in the temperature range 178–186 K, the saturation of magnetization was observed at high fields. This indicates that the sample could transform completely into austenite at 5 T.

When comparing the first and second cycles of $M(H)$ curves, in the temperature range from 178 to 186 K, during increasing the magnetic field, the magnetization in the low-field region of the second cycle was slightly higher than that in the first cycle. This indicated that a small amount of austenite induced in first field cycle was retained and did not transform back into martensite during the decreasing magnetic field in the first cycle. The curve recorded during the decreasing field in the first cycle almost overlapped with that recorded during the decreasing field in the second cycle. In addition, the $M(H)$ curve recorded in the low magnetic field range during the increasing field in the second cycle was consistent with that during the decreasing field in the second cycle. These phenomena indicated that the part of retained austenite (only a tiny portion) after descending field in the first cycle did not participate in the subsequent transformation any more, and thus a reversible transformation between the martensite transformed back in the first cycle and the austenite could happen in the second and subsequent cycles. This is similar to the cases in [23,32]. As a result, a reversible first-order phase transformation, induced by a magnetic field, was achieved in the $Ni_{50}Mn_{34}Fe_3In_{13}$ microwire.

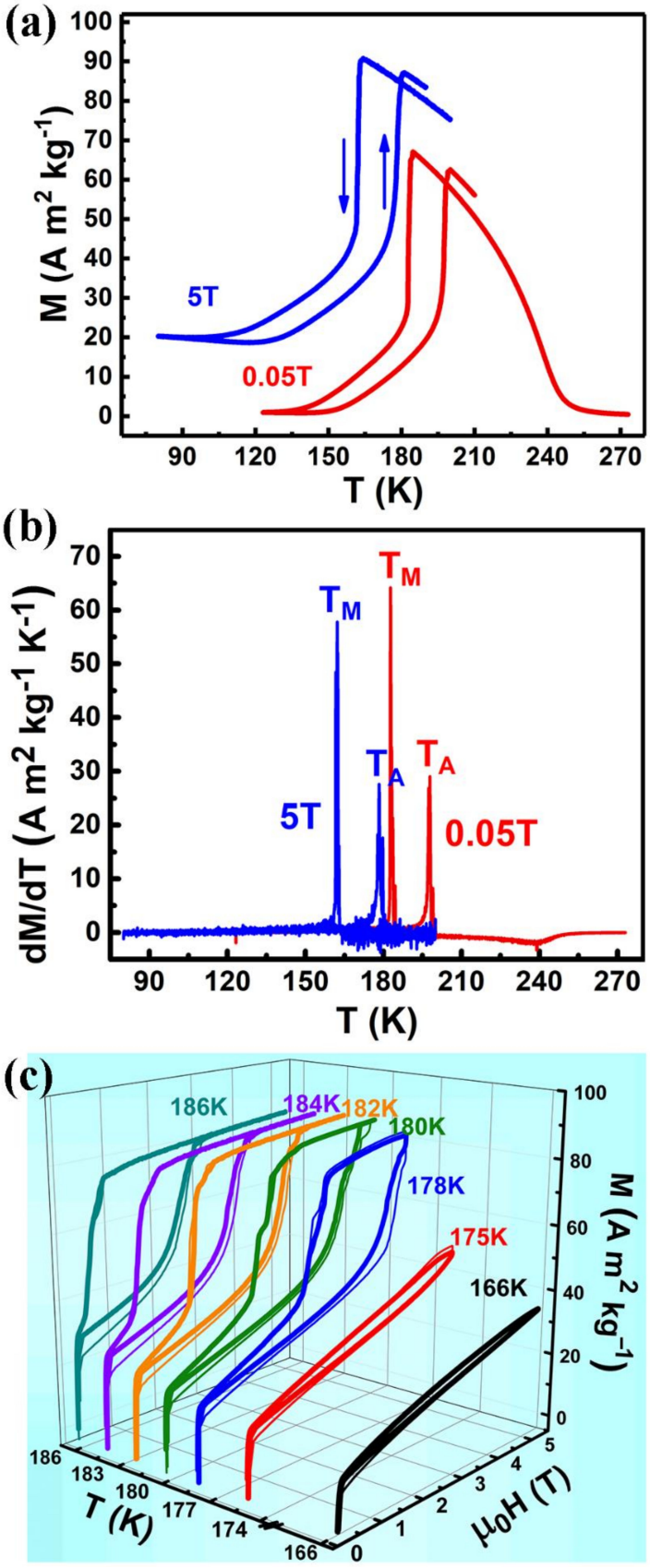

Figure 5. (**a**) $M(T)$ curves measured under 0.05 T and 5 T for the $Ni_{50}Mn_{34}Fe_3In_{13}$ microwire, (**b**) dM/dT derived from the curves in (**a**) shown as a function of temperature and (**c**) $M(H)$ curves measured during the first (thin lines) and second (thick lines) cycles of ascending and descending magnetic fields at different constant temperatures for the $Ni_{50}Mn_{34}Fe_3In_{13}$ microwire.

Magnetically driven multifunctional properties, such as magnetic superelasticity, magnetothermal conductivity, magnetoresistance and magnetocaloric effect, were anticipated in this $Ni_{50}Mn_{34}Fe_3In_{13}$ microwire. This is based on the reversible first-order phase transformation that was induced by a magnetic field. The magnetocaloric effect was estimated as an example of the multifunctional properties mentioned above. The reversible magnetic-field-induced entropy change (ΔS_m) was estimated from the $M(H)$ curves in Figure 5c. In the second cycle, the magnetic-field-induced phase transformation was reversible and, thus, the resultant ΔS_m was reversible as well. Therefore, the $M(H)$ curves in the second cycle were used to compute the reversible ΔS_m.

The critical field $\mu_0 H_{cr}$ for magnetic-field-induced phase transformation, extracted from the $M(H)$ curves in the second cycle, is shown as a function of temperature in Figure 6a. Linear fitting of the $\mu_0 H_{cr}$ vs. T data yielded a slope of -0.237 T/K, which was in accordance with the experimental $\mu_0 \Delta H / \Delta T_A$ value (-0.254 T/K). As a tiny amount of austenite coexists with martensite before applying the magnetic field, the estimation of ΔS_m using the Maxwell relation may lead to spurious results [33]. In contrast, estimation using the Clausius–Clapeyron relation could yield the correct value of ΔS_m even in the case of the coexistence of two phases, since ΔS_m in the Clausius–Clapeyron relation is directly connected to the field-induced magnetization difference at any given temperature. Therefore, it is more suitable to use the Clausius–Clapeyron relation to estimate the reversible ΔS_m. The ΔS_m can be estimated by the following relation [34–36]:

$$\Delta S_m = -\Delta M' \frac{d(\mu_0 H_{cr})}{dT} \quad (2)$$

in which $\Delta M'$ is the magnetization difference between the magnetization values at the final and initial fields. Since the magnetization rapidly changes in the $M(H)$ curves below 0.2 T, which could lead to numerical instabilities, the initial magnetic field selected was 0.2 T. The $d(\mu_0 H_{cr})/dT$ is -0.237 T/K, as mentioned above.

The reversible field-induced entropy change ΔS_m for a magnetic field change from 0.2 T to 5 T at different temperatures is displayed in Figure 6b. It can be seen that an inverse magnetocaloric effect was achieved as the ΔS_m values at all the temperatures are positive. The maximum reversible ΔS_m for a magnetic field change from 0.2 T to 5 T is as high as 15.1 J kg^{-1} K^{-1}, which is higher than that in typical MMSMA microwires [23,33]. The large reversible magnetocaloric effect and high specific surface area confer on the present microwire high potential for magnetic refrigeration applications.

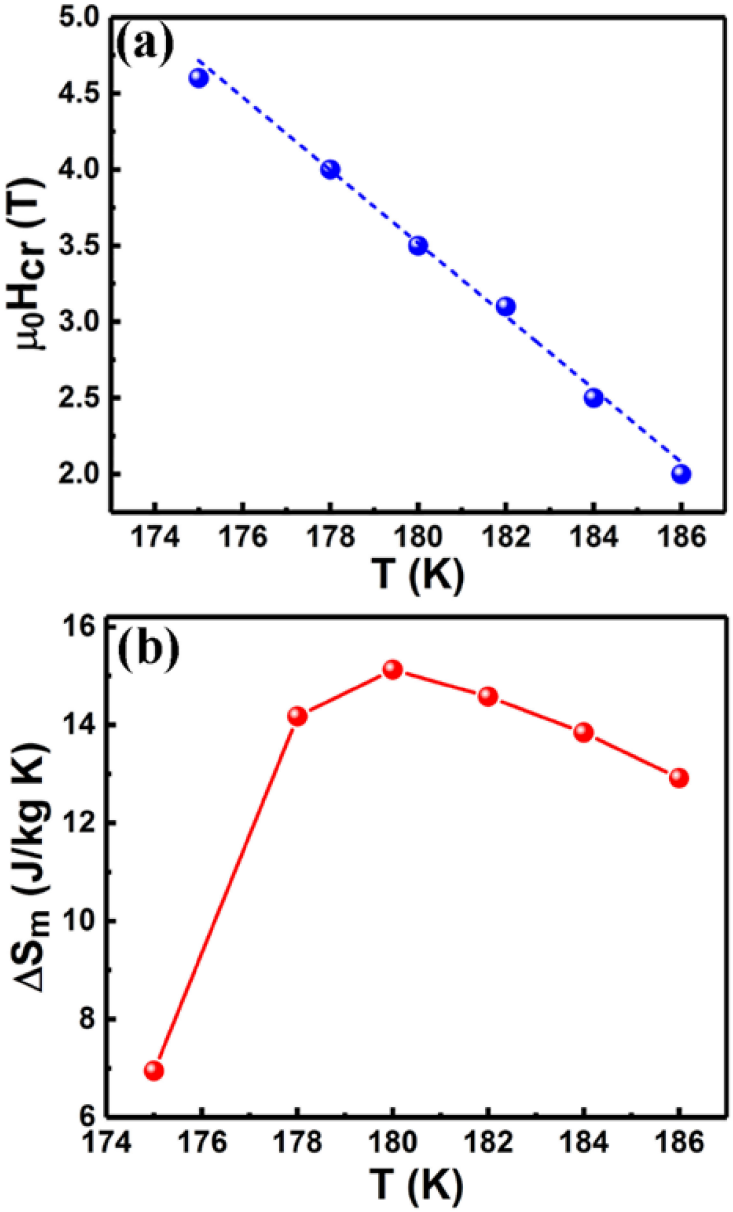

Figure 6. (**a**) Critical magnetic field for magnetic-field-induced phase transformation ($\mu_0 H_{cr}$) that was extracted from the $M(H)$ curves in the second cycle in Figure 5b, shown as a function of temperature for the $Ni_{50}Mn_{34}Fe_3In_{13}$ microwire. The dashed line represents the linear fitting of the data (denoted by symbols). (**b**) Reversible magnetic-field-induced entropy change ΔS_m as a function of temperature for the field change from 0.2 T to 5 T for the $Ni_{50}Mn_{34}Fe_3In_{13}$ microwire.

4. Discussion

The magnetostress is an important property for magnetic actuation applications and it is usually defined as the change in the critical stress for stress-induced martensitic transformation under a given magnetic field [37]. In Ni-Mn-based MMSMAs, since the austenite is ferromagnetic and the martensite is weak magnetic, the magnetic field favors austenite. This leads to austenite stabilization and an increase in critical stress for stress-induced martensitic transformation at a given temperature; the magnetic field and the stress act in opposite directions under simultaneously applied magnetic field and stress.

The Zeeman energy, which arises from the difference between the saturation magnetizations of austenite and martensite, is the driving force for magnetic-field-induced first-order phase transformation [38]. Zeeman energy continuously increases with an increasing magnetic field. Therefore, it is possible to achieve a large output magnetostress

in the present $Ni_{50}Mn_{34}Fe_3In_{13}$ microwire, considering the large magnetization difference between austenite and martensite.

It is possible to predict the magnetostress as a function of applied field if the change in critical stress for stress-induced phase transformation with temperature ($\Delta\sigma/\Delta T$) and the change in transformation temperature with applied field ($\Delta T/\mu_0\Delta H$) are known. The change in stress with applied magnetic field ($\Delta\sigma/\mu_0\Delta H$) can be approximated as follows [37,38]:

$$\frac{\Delta\sigma}{\mu_0\Delta H} = -\frac{\Delta\sigma}{\Delta T} \times \frac{\Delta T}{\mu_0\Delta H}. \quad (3)$$

The $\Delta\sigma/\Delta T$ and $\Delta T_A/\mu_0\Delta H$ for the present $Ni_{50}Mn_{34}Fe_3In_{13}$ microwire are 1.69 MPa/K and −3.94 K/T, respectively, as determined before. With Equation (3), $\Delta\sigma/\mu_0\Delta H$ was estimated to be 6.66 MPa/T for the $Ni_{50}Mn_{34}Fe_3In_{13}$ microwire. Therefore, a large magnetic work output is expected from the present microwire, showing its potential for magnetic actuation applications. Under a magnetic field of 1 T, it is possible to obtain a magnetostress of 6.66 MPa and under 5 T, the magnetostress would be 33.3 MPa.

The present $Ni_{50}Mn_{34}Fe_3In_{13}$ microwire exhibited both magnetic-field-induced phase transformation and stress-induced martensitic transformation. Since stress-induced martensitic transformation occurred between 213 K and 283 K, a considerable elastocaloric effect was anticipated in this temperature range. Based on the magnetic-field-induced transformation, a large reversible magnetocaloric effect was achieved and other magnetoresponsive properties such as magnetic-field-induced strain and magnetoresistance were expected. Owing to the coupling between elastic deformation and magnetization, the elastomagnetic effect [39–41] could also be achieved in the microwire. Since the strain change could be detected by monitoring the change in magnetization, the microwire could also be used in non-contact strain sensors.

5. Conclusions

A Ni-Fe-Mn-In microwire exhibiting giant tensile superelasticity and magnetic-field-induced first-order phase transformation was developed. This $Ni_{50}Mn_{34}Fe_3In_{13}$ microwire shows a giant recoverable strain of more than 20% as a result of stress-induced martensitic transformation in the temperature range of 233–283 K. This represents the highest recoverable strain reported heretofore in Ni-Mn-based SMAs. In addition, the present microwire exhibits a large shape memory effect with a recoverable strain of up to 13.9% under a constant tensile stress of 225 MPa. These properties contrast with those in the bulk MMSMAs that barely show any tensile deformability. Due to the considerable magnetization difference between martensite and austenite, magnetic-field-induced first-order phase transformation is realized in this microwire. Thus, a series of magneto-responsive properties were anticipated. Indeed, a large reversible magnetocaloric effect, with an isothermal entropy change ΔS_m of 15.1 J kg^{-1} K^{-1} for a field change from 0.2 T to 5 T, was obtained from this microwire. The achievement of magnetic-field and stress-induced transformations confers on this $Ni_{50}Mn_{34}Fe_3In_{13}$ microwire great potential for application in miniature multifunctional devices.

Author Contributions: Conceptualization, D.C. and Z.C.; methodology, Z.C., S.L. (Shilei Li) and Y.Z.; validation, Z.C., D.C., S.L. (Shilei Li), Y.W. and Y.R.; formal analysis, Z.C., Y.Z., Y.C., S.L. (Shaohui Li) and C.S.; investigation, Z.C., Y.Z., and S.L. (Shengwei Li); writing—original draft preparation, Z.C.; writing—review and editing, D.C. and Z.C. All authors have read and agreed to the published version of the manuscript.

Funding: Financial support from the National Natural Science Foundation of China (Nos. 51731005, 51822102, 52031005, 51831003 and 51527801) and the Fundamental Research Funds for the Central Universities (No. FRF-TP-18-008C1) is gratefully acknowledged. This work is also supported by the Funds for Creative Research Groups of China (No. 51921001). Use of the Advanced Photon Source was supported by the U.S. Department of Energy, Office of Science, Office of Basic Energy Science, under Contract No. DE-AC02-06CH11357.

Data Availability Statement: The data that support the findings of this study are available from the corresponding author, upon reasonable request.

Conflicts of Interest: The authors declare no conflict of interest.

References

1. Otsuka, K.; Wayman, C.M. *Shape Memory Materials*; Cambridge University Press: Cambridge, UK, 1998.
2. Jani, J.M.; Leary, M.; Subic, A.; Gibson, M.A. A review of shape memory alloy research, applications and opportunities. *Mater. Des.* **2014**, *56*, 1078–1113. [CrossRef]
3. Sun, L.; Huang, W.M.; Ding, Z.; Zhao, Y.; Wang, C.C.; Purnawali, H.; Tang, C. Stimulus-responsive shape memory materials: A review. *Mater. Des.* **2012**, *33*, 577–640. [CrossRef]
4. Manjaiah, M.; Narendranath, S.; Basavarajappa, S. Review on non-conventional machining of shape memory alloys. *Trans. Nonferrous Met. Soc. China* **2014**, *24*, 12–21. [CrossRef]
5. Wu, M.H.; Schetky, L. Industrial Applications for Shape Memory Alloys. In Proceedings of the International Conference on Shape Memory and Superelastic Technologies, Pacific Grove, CA, USA, 30 April–4 May 2000; pp. 171–182.
6. Stoeckel, D. Shape memory actuators for automotive applications. *Mater. Des.* **1990**, *11*, 302–307. [CrossRef]
7. Velmurugan, C.; Senthilkumar, V.; Dinesh, S.; Arulkirubakaran, D. Review on phase transformation behavior of NiTi shape memory alloys. *Mater. Today Proc.* **2018**, *5*, 14597–14606. [CrossRef]
8. Choudhary, N.; Kaur, D. Shape memory alloy thin films and heterostructures for MEMS applications: A review. *Sens. Actuators A* **2016**, *242*, 162–181. [CrossRef]
9. Petrini, L.; Migliavacca, F. Biomedical applications of shape memory alloys. *J. Met.* **2011**, *2011*, 501483. [CrossRef]
10. Krenke, T.; Duman, E.; Acet, M.; Wassermann, E.F.; Moya, X.; Mañosa, L.; Planes, A.; Suard, E.; Ouladdiaf, B. Magnetic superelasticity and inverse magnetocaloric effect in Ni-Mn-In. *Phys. Rev. B* **2007**, *75*, 104414. [CrossRef]
11. Mañosa, L.; Moya, X.; Planes, A.; Aksoy, S.; Acet, M.; Wassermann, E.; Krenke, T. Magnetostrain in Multifunctional Ni-Mn Based Magnetic Shape Memory Alloys. *Mater. Sci. Forum* **2008**, *583*, 111–117. [CrossRef]
12. Kainuma, R.; Imano, Y.; Ito, W.; Sutou, Y.; Morito, H.; Okamoto, S.; Kitakami, O.; Oikawa, K.; Fujita, A.; Kanomata, T.; et al. Magnetic-field-induced shape recovery by reverse phase transformation. *Nature* **2006**, *439*, 957–960. [CrossRef]
13. Pathak, A.K.; Dubenko, I.; Pueblo, C.; Stadler, S.; Ali, N. Magnetoresistance and magnetocaloric effect at a structural phase transition from a paramagnetic martensitic state to a paramagnetic austenitic state in $Ni_{50}Mn_{36.5}In_{13.5}$ Heusler alloys. *Appl. Phys. Lett.* **2010**, *96*, 172503. [CrossRef]
14. Huang, L.; Cong, D.Y.; Ma, L.; Nie, Z.H.; Wang, Z.L.; Suo, H.L.; Ren, Y.; Wang, Y.D. Large reversible magnetocaloric effect in a Ni-Co-Mn-In magnetic shape memory alloy. *Appl. Phys. Lett.* **2016**, *108*, 032405. [CrossRef]
15. Liu, J.; Woodcock, T.G.; Scheerbaum, N.; Gutfleisch, O. Influence of annealing on magnetic field-induced structural transformation and magnetocaloric effect in Ni-Mn-In-Co ribbons. *Acta Mater.* **2009**, *57*, 4911–4920. [CrossRef]
16. Liu, J.; Gottschall, T.; Skokov, K.P.; Moore, J.D.; Gutfleisch, O. Giant magnetocaloric effect driven by structural transitions. *Nat. Mater.* **2012**, *11*, 620–626. [CrossRef]
17. Ueland, S.M.; Chen, Y.; Schuh, C.A. Oligocrystalline Shape Memory Alloys. *Adv. Funct. Mater.* **2012**, *22*, 2094–2099. [CrossRef]
18. Dunand, D.C.; Müllner, P. Size effects on magnetic actuation in Ni-Mn-Ga shape-memory alloys. *Adv. Mater.* **2011**, *23*, 216–232. [CrossRef]
19. Juan, J.S.; Nó, M.L.; Schuh, C.A. Superelasticity and Shape Memory in Micro- and Nanometer-scale Pillars. *Adv. Mater.* **2008**, *20*, 272–278. [CrossRef]
20. Chiriac, H.; Óvári, T.A. Amorphous glass-covered magnetic wires: Preparation, properties, applications. *Prog. Mater. Sci.* **1996**, *40*, 333–407. [CrossRef]
21. Vázquez, M.; Chiriac, H.; Zhukov, A.; Panina, L.; Uchiyama, T. On the state-of-the-art in magnetic microwires and expected trends for scientific and technological studies. *Phys. Status Solidi A* **2011**, *208*, 493–501. [CrossRef]
22. Qian, M.F.; Zhang, X.X.; Witherspoon, C.; Sun, J.F.; Müllner, P. Superelasticity and shape memory effects in polycrystalline Ni-Mn-Ga microwires. *J. Alloys Compd.* **2013**, *577*, S296–S299. [CrossRef]
23. Chen, Z.; Cong, D.; Sun, X.; Zhang, Y.; Yan, H.; Li, S.; Li, R.; Nie, Z.; Ren, Y.; Wang, Y. Magnetic field-induced magnetostructural transition and huge tensile superelasticity in an oligocrystalline Ni–Cu–Co–Mn–In microwire. *IUCrJ* **2019**, *6*, 843–853. [CrossRef]
24. Li, F.Q.; Qu, Y.H.; Yan, H.L.; Chen, Z.; Cong, D.Y.; Sun, X.M.; Li, S.H.; Wang, Y.D. Giant tensile superelasticity originating from two-step phase transformation in a Ni-Mn-Sn-Fe magnetic microwire. *Appl. Phys. Lett.* **2018**, *113*, 112402. [CrossRef]
25. Kraus, W.; Nolze, G. POWDER CELL–a program for the representation and manipulation of crystal structures and calculation of the resulting X-ray powder patterns. *J. Appl. Crystallogr.* **1996**, *29*, 301–303. [CrossRef]
26. Song, Y.T.; Chen, X.; Dabade, V.; Shield, T.W.; James, R.D. Enhanced reversibility and unusual microstructure of a phase-transforming material. *Nature* **2013**, *502*, 85–88. [CrossRef]
27. Hane, K.F.; Shield, T.W. Microstructure in the cubic to monoclinic transition in titanium-nickel shape memory alloys. *Acta Mater.* **1999**, *47*, 2603–2617. [CrossRef]
28. Liang, X.; Xiao, F.; Jin, M.; Jin, X.; Fukuda, T.; Kakeshita, T. Elastocaloric effect induced by the rubber-like behavior of nanocrystalline wires of a Ti-50.8Ni (at.%) alloy. *Scr. Mater.* **2017**, *134*, 42–46. [CrossRef]
29. Ma, J.; Karaman, I.; Noebe, R.D. High temperature shape memory alloys. *Int. Mater. Rev.* **2011**, *55*, 257–315. [CrossRef]

30. Kustov, S.; Corró, M.L.; Pons, J.; Cesari, E. Entropy change and effect of magnetic field on martensitic transformation in a metamagnetic Ni-Co-Mn-In shape memory alloy. *Appl. Phys. Lett.* **2009**, *94*, 191901. [CrossRef]
31. Cong, D.Y.; Roth, S.; Schultz, L. Magnetic properties and structural transformations in Ni-Co-Mn-Sn multifunctional alloys. *Acta Mater.* **2012**, *60*, 5335–5351. [CrossRef]
32. Qu, Y.H.; Cong, D.Y.; Chen, Z.; Gui, W.Y.; Sun, X.M.; Li, S.H.; Ma, L.; Wang, Y.D. Large and reversible inverse magnetocaloric effect in $Ni_{48.1}Co_{2.9}Mn_{35.0}In_{14.0}$ metamagnetic shape memory microwire. *Appl. Phys. Lett.* **2017**, *111*, 192412. [CrossRef]
33. Liu, G.J.; Sun, J.R.; Shen, J.; Gao, B.; Zhang, H.W.; Hu, F.X.; Shen, B.G. Determination of the entropy changes in the compounds with a first-order magnetic transition. *Appl. Phys. Lett.* **2007**, *90*, 032507. [CrossRef]
34. Balli, M.; Fruchart, D.; Gignoux, D.; Zach, R. The "colossal" magnetocaloric effect in $Mn_{1-x}Fe_xAs$: What are we really measuring? *Appl. Phys. Lett.* **2009**, *95*, 072509. [CrossRef]
35. Qu, Y.H.; Cong, D.Y.; Sun, X.M.; Nie, Z.H.; Gui, W.Y.; Li, R.G.; Ren, Y.; Wang, Y.D. Giant and reversible room-temperature magnetocaloric effect in Ti-doped Ni-Co-Mn-Sn magnetic shape memory alloys. *Acta Mater.* **2017**, *134*, 236–248. [CrossRef]
36. Szymczak, R.; Nedelko, N.; Lewińska, S.; Zubov, E.; Sivachenko, A.; Gribanov, I.; Radelytskyi, I.; Dyakonov, K.; Ślawska-Waniewska, A.; Valkov, V.; et al. Comparison of magnetocaloric properties of the $Mn_{2-x}Fe_xP_{0.5}As_{0.5}$ (x = 1.0 and 0.7) compounds. *Solid. State Sci.* **2014**, *36*, 29–34. [CrossRef]
37. Karaca, H.E.; Karaman, I.; Basaran, B.; Ren, Y.; Chumlyakov, Y.I.; Maier, H.J. Magnetic Field-Induced Phase Transformation in NiMnCoIn Magnetic Shape-Memory Alloys-A New Actuation Mechanism with Large Work Output. *Adv. Funct. Mater.* **2009**, *19*, 983–998. [CrossRef]
38. Turabi, A.S.; Karaca, H.E.; Tobe, H.; Basaran, B.; Aydogdu, Y.; Chumlyakov, Y.I. Shape memory effect and superelasticity of NiMnCoIn metamagnetic shape memory alloys under high magnetic field. *Scr. Mater.* **2016**, *111*, 110–113. [CrossRef]
39. Ausanio, G.; Hison, C.; Iannotti, V.; Luponio, C.; Lanotte, L. Elastomagnetic effect in novel elastic magnets. *J. Magn. Magn. Mater.* **2004**, *272–276*, 2069–2071. [CrossRef]
40. Lanotte, L.; Ausanio, G.; Iannotti, V.; Pepe, G.; Carotenuto, G.; Netti, P.; Nicolais, L. Magnetic and magnetoelastic effects in a composite material of Ni microparticles in a silicone matrix. *Phys. Rev. B* **2001**, *63*, 811–820. [CrossRef]
41. Tanaka, Y.; Himuro, Y.; Kainuma, R.; Sutou, Y.; Omori, T.; Ishida, K. Ferrous Polycrystalline Shape-Memory Alloy Showing Huge Superelasticity. *Science* **2010**, *327*, 1488–1490. [CrossRef]